ORIGINAL PAPER

Observation of bubble layer formed on hydrogen and oxygen gas-evolving electrode in a magnetic field

Hisayoshi Matsushima · Takami Iida ·
Yasuhiro Fukunaka

Abstract The evolution of hydrogen and oxygen gasses in a 0.36-M KOH electrolyte was observed in a magnetic field, and the void fraction was calculated by a hydrodynamic model. Both gasses evolving on a platinum working electrode formed a bubble layer which increased the ohmic resistance. In addition to natural convection, magnetohydrodynamic (MHD) convection in a magnetic field improved the electrolytic conductivity by supplying a fresh solution (pumping effect) and removing gas bubbles. The MHD convection reduced the void fraction of hydrogen gas more than that of oxygen, which can be explained by the poor wettability of the oxygen evolving electrode.

Keywords Magnetic field · Water electrolysis · Void fraction · Hydrogen gas bubble · Oxygen gas bubble

Introduction

Water electrolysis has attracted much attention due to fundamental electrochemistry [1, 2]. It plays an important role in the development of soda electrolysis and alumina refinement, so-called mature industries. The desire of a low carbon emission society has now put electrolysis engineering in the limelight. The electrolysis producing both hydrogen and oxygen gasses can be applied to a clean energy storage/conversion system [3, 4]. Furthermore, it is expected to be used as a micro-actuator using a nano-bubble [5, 6].

The analysis of gas bubble evolution is still a challenging topic due to the intrinsic phenomena. The key issue leading a highly efficient electrolysis is strongly connected to the control of the gas bubble evolution. It is characterized by the wettability among the three phase interfaces (solid/gas/liquid phases). The bubble growth and detachment cause some microscopic convections on the electrode surface [7, 8] as well as an upstream natural one due to buoyancy (pumping effect) [9–13]. These convections enhance the mass transfer of the dissolved gas and ionic species. On the other hand, gas bubbles adhering on the electrode reduce the reaction area [14–17] and dispersing bubbles into the electrolyte creates a void area [18–22] that increases the ohmic resistance between the cathode and anode.

Some research groups have recently reported unique approaches in order to overcome the negative factor by the bubble. Polymer electrode membrane electrolysis is one of the reasonable ways to solve the void problem, although the conductivity and durability are still a concern [23–25]. The other possibility is the utilization of an ultra-hydrophilic (or hydrophobic) electrode assembly using a nano-wire array [26–28]. Zhu et al. reported interesting phenomena such that the contact angle among the three phases changes depending on the nanoscale surface roughness [28]. We believe that the hydrophilic wire array is a good material for accelerating the bubble detachment in order to maintain the active electrode area.

The gas evolution is analyzed by changing the external environment, e.g., magnetic field [29–33], microgravity [34–38], ultrasonic superimposition [39], and centrifugal field [40, 41]. We operated the water electrolysis under a

H. Matsushima (✉)
Interdisciplinary Graduate School of Medicine and Engineering,
University of Yamanashi,
4-3-11 Takeda,
Kofu 400-8511, Japan
e-mail: hisayoshim@yamanashi.ac.jp

T. Iida · Y. Fukunaka
Graduate School of Energy Science, Kyoto University,
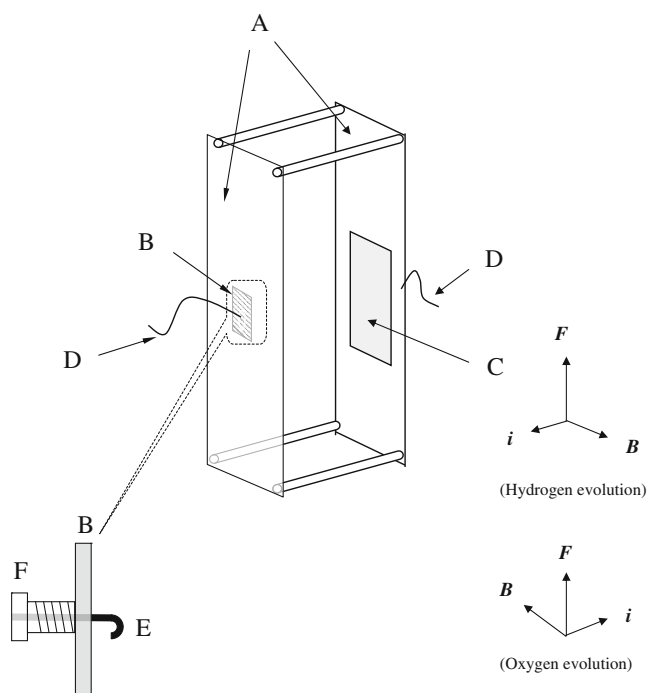Sakyo-ku,
Kyoto 606-8501, Japan

Fig. 1 Schematic diagram of experimental cell. *A*, plastic cell (30× 10×5 mm³); *B*, working electrode (Pt, 4×7×0.1 mm³); *C*, counter electrode (Pt, 11×7×0.1 mm³); *D*, contacting wire; *E*, Luggin probe; *F*, plastic screw

high magnetic field (~5 T) and reported that the cell voltage remarkably decreased from 3.8 V to 3.3 V at 1.5 A cm⁻² [33] when the interelectrode distance was 5 mm. This improvement was explained by the magneto-hydrodynamic (MHD) convection induced by the Lorenz force. The sticking and dispersing of the gas bubbles were forcedly removed by the MHD convection as an additional pumping effect, which became more noticeable with the increasing current density. Moreover, Koza et al. reported that the distorted electric lines of force around the gas bubble created a vortex convection (microscopic MHD) that helped with bubble detachment [31]. Although many interesting results obtained in a magnetic field have been published, the qualitative analysis of the gas-evolving electrode has not been investigated very much because of the difficulty of in situ observations in a high magnetic field.

Based on previous studies [33], the present paper is the first study to carry out in situ observations of the bubble dispersion layer using a high-speed camera and try to quantitatively analyze of the gas evolution by calculating the void fraction in a magnetic field.

Experimental

Figure 1 shows a schematic drawing of the electrode arrangement. Three electrodes were fixed in the cell holder which was placed in a rectangular glass cuvet maintained at

298 K. The working (0.28 cm²) and counter electrodes (0.77 cm²) were platinum sheets (Nilaco Corp., 99.99%). Their surfaces were polished using a no. 4000 grade emery paper and subsequently rinsed with a nitric acid solution. The reference electrode was Ag/AgCl. It was connected to a Luggin probe mounted in the working electrode in order to not disturb the MHD convection. The distance between the probe and the working electrode could be adjusted by the plastic screw. The electrolyte was a 0.36-M KOH aqueous solution prepared from KOH pellets (Kanto Kagaku, UGR) and ultra-pure water

The electrochemical studies of the gas-evolving electrode were conducted by a computer-controlled potentiostat (Hokuto Denkou Corp., HZ-3000). IR-drop was measured by the current interrupter technique.

A static and uniform magnetic field (~5 T) was generated by a super-conducting magnet (Sumitomo Heavy Ind., HF5-100VHF). It was applied perpendicular to the electrode surface in order to induce an upward MHD convection as indicated in Fig. 1. To observe the gas motion in the magnetic field, a special optical arrangement employing a parallel light was used (Fig. 2). The gas evolution was recorded by a high-speed camera (Phantom, V7) with 2,000 frames/s.

Results and discussion

The water electrolysis was run for 60 s in order to reach a stable condition. The images of the high-speed camera clearly demonstrated the transient behavior of the gas evolution at the moment when the electrolysis was started. Figure 3 shows the typical sequence of the video images (0.05~0.4 s) when a cathodic current (−1.6 A cm⁻²) is applied to the working electrode at (a) 0 T and (b) 5 T. In the absence of the magnetic field, many hydrogen bubbles were created on the working electrode and then some of the
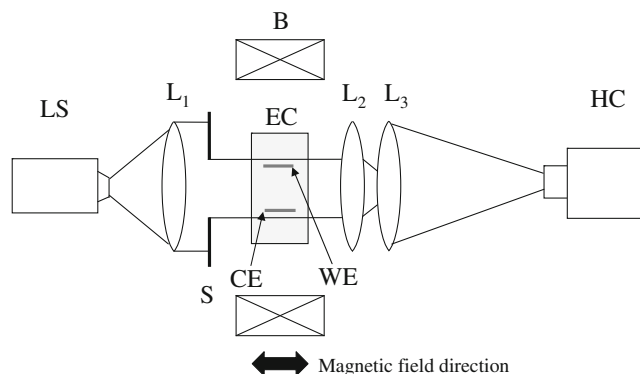

Fig. 2 Top view of optical arrangement for measuring bubble layer. *LS* light source, *L₁–L₃* lens, *S* slit, *EC* electrolytic cell, *CE* counter electrode, *WE* working electrode, *HC* high-speed camera)

Fig. 3 Transient image of gas evolution behavior in **a** no magnetic field, and **b** a magnetic field of 5 T at measurement time of *i* 0.05 s, *ii* 0.15 s, *iii* 0.3 s and *iv* 0.5 s. Electrolyte, 0.36 M KOH, current density, −1.0 A cm⁻²
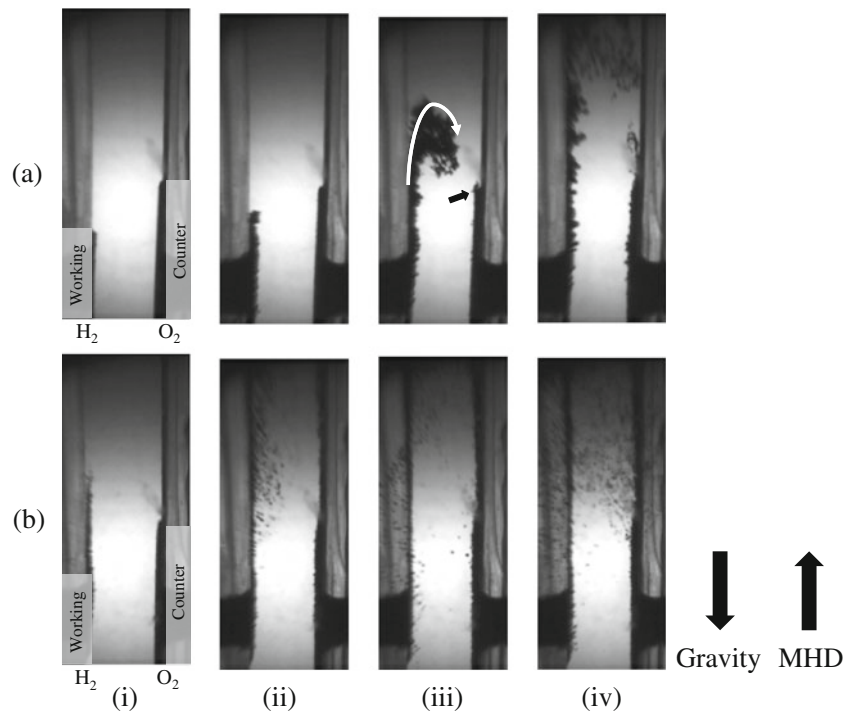
bubbles began to detach from the surface within 0.15 s. Along the cell holder, they formed a bubble curtain thus inducing a natural convection (Fig. 3a (ii)).

The top part of the bubble curtain began to swirl like a blown up smoke (Fig. 3a (iii)). The vortex formation suggests the intrinsic velocity profile of the curtain layer. That is, the velocity at the interface between the bubble layer and the bulk electrolyte is slowed by the friction resistance. Moreover, the inner bubbles rolling on the electrode and the cell holder can stream more smoothly than outer ones in the dispersion layer. The finer bubbles reached the top surface and then formed a stable bubble layer after 0.5 s (Fig. 3a (iv)).

Oxygen bubbles on the counter electrode took a longer time to be observed (0.3 s) than the hydrogen ones due to the larger electrode area. A few bubbles began to aggregate

with each other and detach from the electrode surface as indicated by the arrow (Fig. 3a (iv)). The picture showed that the size of the gas bubble forming the oxygen layer was finer than the hydrogen one, which was different from the results of a previous study [36, 37]. Some of the gas bubbles evolved from the electrode edge rather than the surface. This was probably because the edge side of the counter electrode was not partially covered by epoxy resin, and fine bubbles were created there. A small number of the oxygen gas caused laminar natural convection without any vortex.

In a magnetic field, an upstream MHD convection was induced by the Lorenz force as soon as the electrolysis started. Figure 3b (i) shows that hydrogen bubbles evolving from the working electrode formed a very thin bubble layer within 0.05 s. A more detailed study about the transient

Fig. 4 Thickness of bubble layer (δ) at **a** hydrogen and **b** oxygen gas-evolving electrodes in various magnetic fields at a current density of 0.1 A cm⁻² (*circles*), 0.3 A cm⁻² (*triangles*), 0.6 A cm⁻² (*inverted triangles*), 1.0 A cm⁻² (*squares*). Electrolyte, 0.36 M KOH
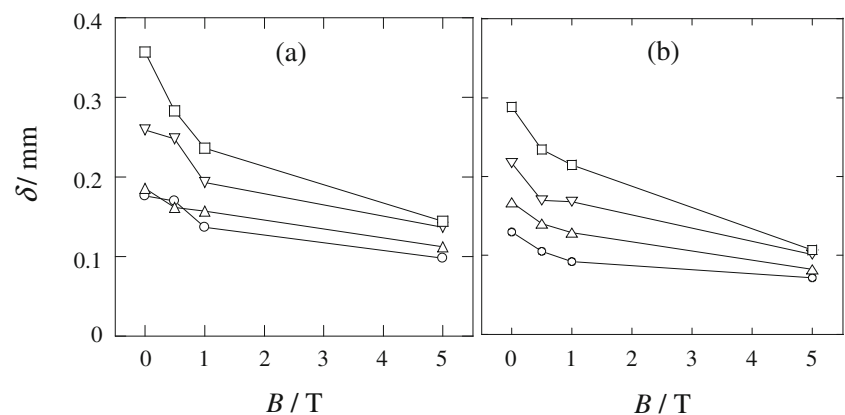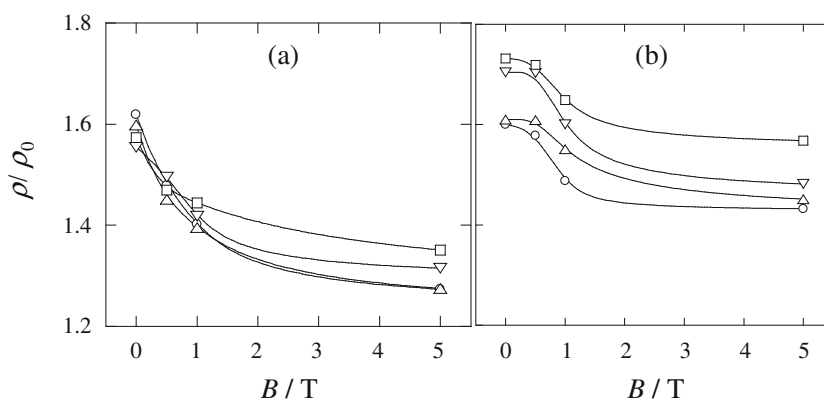
Fig. 5 Relative value (ρ/ρ_0) of the electrolytic resistivity (ρ) containing gas bubbles of **a** hydrogen and **b** oxygen as compared with that (ρ_0) of the free electrolyte in various magnetic fields at a current density of 0.1 A cm^{-2} (*circles*), 0.3 A cm^{-2} (*triangles*), 0.6 A cm^{-2} (*inverted triangles*), 1.0 A cm^{-2} (*squares*). Electrolyte, 0.36 M KOH

phenomena of MHD convection shorter than 0.05 s will be presented by the analysis of the high-speed camera images. Some of bubbles detaching from the working electrode remarkably scattered in the bulk solution (Fig. 3b (ii)), but they did not vortex as seen in no magnetic field. The high-speed movie demonstrated that the bubbles moved by both the MHD and natural convection rebounded at the top and then went downward at the outer side of the cell holder. Therefore, many bubbles could be observed on the backside of the working electrode (Fig. 3b (iii)). Hydrogen and oxygen bubbles were mixture by the turbulent flow at the liquid/air interface at 0.5 s. One third of the electrolyte from the top side turned milky in color due to the many fine bubbles formed during the electrolysis operation.

In contrast to taking a longer time to form an oxygen bubble layer in the no magnetic field, a thin bubble layer could be pictured at 0.15 s. The bubble size of oxygen seemed as small as the hydrogen one, although the precise measurement was difficult because of the optical arrangement focusing only on the measurement of the dispersion layer and the convectional effects.

The bubble evolution became stable at 10 s after the electrolysis was started. The cathodic and anodic constant currents ($i=\pm0.1\sim\pm1.0$ A cm^{-2}) were applied to the working electrode to study the bubble evolutions of hydrogen and oxygen gasses, respectively. The thickness (δ) of the bubble layer of the hydrogen and oxygen gasses at the center of the working electrode was measured in Fig. 4. The thickness of both layers increased with the increasing current density. Some plots of the data, e.g., 0.1 and 0.3 A cm^{-2} in Fig. 4a, did not show the MHD effect, which might be experimental error. The faster MHD convection reduced the thickness more in the high current region.

The hydrogen bubbles were more dispersed into the bulk than the oxygen ones, regardless of the magnetic field intensity. This was attributed to the larger gas volume of hydrogen. Moreover, a more detailed observation by the high-speed movie demonstrated that the hydrogen bubbles spontaneously jumped normal to the electrode, which was

similar to the gas motion in a microgravity environment [38]. The hydrogen bubble was moved by the thermal [42, 43] or concentration (dissolved H_2 gas molecular) [44] capillary effect which induced a microscopic convection flowing from the top to the bottom of a bubble. The microscopic stream could help the jump motion by attacking the junction between the bubbles and the electrode. On the other hand, the oxygen bubbles always adhered to the surface. The platinum surface covered with a thin oxide film has a good affinity for the oxygen molecule, therefore, which keeps oxygen bubble staying on the surface by large adhesion force, although the capillary convection is generated around the oxygen bubbles as well as hydrogen ones.

The current interrupter method can determine the electrolytic resistivity between the reference and working electrode by measuring the ohmic resistance [36]. Figure 5 shows the relative resistivity (ρ/ρ_0) of the electrolyte containing the gas bubbles (ρ) as compared with the free electrolyte (ρ_0). The resistivity of hydrogen depended on
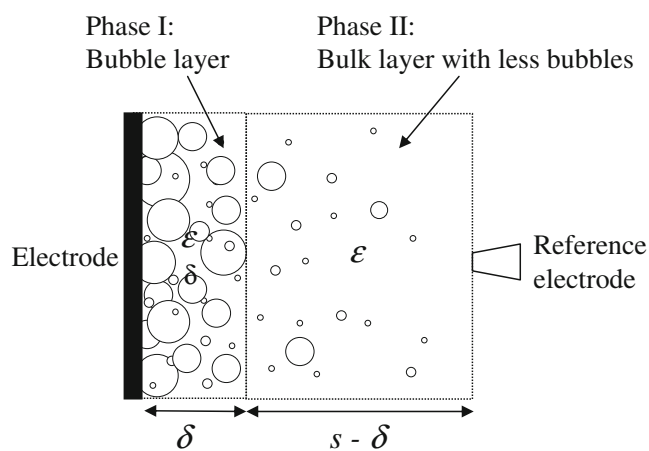

Fig. 6 Model of gas bubble distribution between the working and reference electrodes. ε void fraction of bubble dispersion layer, ε_δ void fraction of bubble layer, δ thickness of bubble layer, s distance between working and reference electrodes

Fig. 7 Dependence of relative resistivity (ρ/ρ_0) on the flow rate ratio of gas volume to liquid (V_L/V_G) at **a** hydrogen and **b** oxygen evolving electrodes in various magnetic fields of 0.5 T (*triangles*), 1 T (*inverted triangles*) and 5 T (*squares*). Electrolyte, 0.36 M KOH; *solid lines* are fitted by Eq. 1
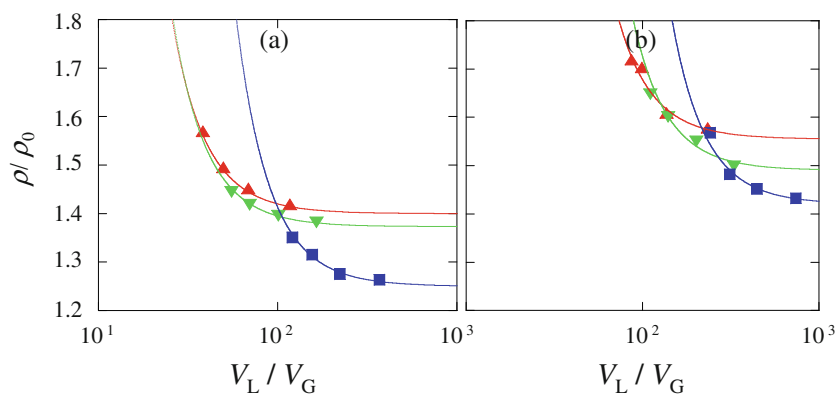
the magnetic field (MHD convection) rather than the current density, which is different from the oxygen results. The MHD convection as an additional pumping effect can improve the conductivity, but the effect seemed to be limited in the high magnetic field. This corresponded to the layer thickness which was sufficiently compressed at the high field intensity as seen in Fig. 4.

The applied current density affects the resistivity as both positive and negative factors. Contrary to the hydrogen bubble easily detaching and rolling on the platinum that can induce both macro- (natural) and microscopic [7] convections to accelerate the mass transfer, oxygen bubbles with a poor wettability are likely to cover and adhere to the surface. At 0 and 0.5 T, in which the convectional effect could be less than that of the surface factor, the reduction in the resistivity on the oxygen evolving electrode was hardly seen, although we still do not know the reason why the resistivity drops only around 1 T independent of the current density.

In a previous study, we calculated the void fraction of the bubble layer in a microgravity environment [36]. The boundary between the bubble layer and the bulk solution can be clearly separated because there are no macroscopic convections dispersing the gas bubbles toward the bulk side. However, the natural and MHD convections distort the ideal situation and distribute the bubbles non-uniformly as shown in Fig. 6 in which the bubble density becomes more enriched closer to the electrode. Dr. Vogt paid attention to the difference in the flow velocity and bubble population between the bubble layer and the bulk part. He proposed a mathematical model for calculating the ohmic resistance of the two parts of the gas dispersion layer; i.e., the bubble layer at the electrode being enriched in gas (phase I) and the bulk flow with a lower bubble population (phase II) [45]. In the present study, we used his model for evaluating the effect of the MHD convection on the void fraction of the two phases. Although the flow velocity during natural convection should be considered, we neglected the effect and focused only on the results obtained in the magnetic field in order to simplify the discussion.

The resistivity measured by the current interrupter method is the sum of the mean resistivities of the two phases. The following equation based on the hydrodynamic model by Vogt [44] is able to calculate the resistivity (ρ_δ) of the bubble layer.

$$\frac{\rho}{\rho_0} = 0.4 \times \left(1 - \frac{\delta}{s}\right) \times \alpha \frac{V_G}{V_L}\left[\left(1 + \alpha\frac{V_G}{V_L}\right)^{2.5} - 1\right] + \frac{\rho_\delta}{\rho_0}\frac{\delta}{s} \quad (1)$$

where s is the distance between the working and reference ($s = 0.5$ mm), and δ is the thickness of the bubble layer. The relative velocity, $a = (v_L/v_G)$, the gas velocity to the liquid one ratio is calculated from the direct measurement (v_G) by the high-speed camera and the Navier–Stokes equation $\left(v_L = \sqrt{2Bil/\sigma}\right)$ where B is the magnetic flux density, σ is the electrolyte density, and L is the length of the working electrode. The ratio (V_G/V_L) of the gas production volume at the working electrode as compared with the bulk flow one is obtained as follows:

$$V_G = \left(\frac{i}{nF}\right)\left(\frac{RT}{p}\right)LH \quad (2)$$
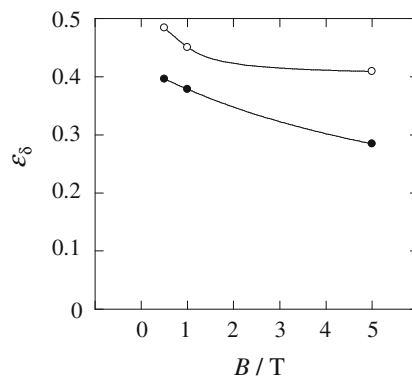
$$V_L = sHv_L \quad (3)$$

Fig. 8 Void fraction (ε_d) of bubble layer at (*empty circles*) oxygen and (*filled squares*) hydrogen gas-evolving electrodes in various magnetic fields

where n is a stoichiometric number, p is the gas pressure, and H is the width of the electrode.

The relative resistivity vs. V_L/V_G is plotted in Fig. 7. The range of V_L/V_G in the magnetic field is around $10^2 \sim 10^3$, which is much higher than that ($10^0 \sim 10^1$) in the non-magnetic field. This supports that the effect of natural convection in the present study could be neglected as already discussed. On the other hand, the range of the relative resistivity showed a reasonable value as reported in the previous study [45]. The present results of both gasses show a lower resistivity at the higher ratio of V_L/V_G. The bulk fluid (V_L) reduces the resistivity by supplying fresh electrolyte and removing the gas bubbles, contrary to the gas production volume (V_G) which increases the gas coverage and the void fraction as a negative factor. Compared with the hydrogen plots, the oxygen had a higher resistivity over a wider range.

The experimental results were well fitted to the solid curves of Eq. 1 as indicated in Fig. 7. The relative resistivity, ρ_δ/ρ_0, gives the void fraction of the bubble curtain layer (ε_δ) according to the Bruggeman equation,

$$\varepsilon_\delta = 1 - \left(\frac{\rho_\delta}{\rho_0}\right)^{1.5} \tag{4}$$

The less coalescesing hydrogen bubbles are small and fine particles, which leads to a lower void fraction than the oxygen one as seen in Fig. 8 due to the existence of many conductive passes among the bubbles. The MHD convection reduced the density of the gas bubbles. The effect of the MHD convection was clearer for the hydrogen evolution. On the other hand, the void fraction of the oxygen one seemed to be saturated (at more than 3 T), which might be attributed to the surface coverage by the poor wettability. The MHD convection compresses the thickness of the bubble curtain layer and increases the bubble density, while it supplies the bubble-free electrolyte from the bottom side of the electrode. The present results suggest that the latter is the dominant effect by the MHD convection to reduce the bubble void for both gas evolutions.

Conclusions

Water electrolysis was investigated in a magnetic field (0~5 T) for the development of a high-efficiency electrolyzer. The bubble layer formed on a platinum working electrode created the void fraction and increased the ohmic resistance. MHD convection was confirmed as a promising technique to reduce the ohmic resistance, because it could remove the gas bubble and supply the bubble-free electrolyte as well as the natural convection. The hydrodynamic model proposed by Vogt made it possible to quantitatively

analyze the void fraction of the bubble layer in a magnetic field. It decreased from 0.40 to 0.28 for the hydrogen bubbles and from 0.48 to 0.41 for the oxygen ones. Compared with the hydrogen bubble, the oxygen one was likely to stick to the electrode surface and actively coalesce due to its poor wettability, even when it was exposed to a fast MHD convection.

References

1. Zeng K, Zhang DK (2010) Prog Energ Combust 36:307–326
2. Wendt H, Imarisio G (1988) J Appl Electrochem 18:1–14
3. Roziere J, Jones DJ (2003) Annu Rev Mater Res 33:503–555
4. Mitlitsky F, Myers B, Weisberg AH (1998) Energ Fuel 12:56–71
5. Chan SC, Chen CR, Liu CH (2010) Sens Actuator A-Phys 163:501–509
6. Van Den Broek DM, Elwenspoek M (2008) Sens Actuator A-Phys 145:387–393
7. Vogt H (1993) Electrochim Acta 38:1421–1426
8. Vogt H (1993) Electrochim Acta 38:1427–1431
9. Mandin P, Wuthrich R, Roustan H (2010) AICHE J 56:2446–2454
10. Mandin Ph, Ait Aissa A, Roustan H, Hamburger J, Picard G (2008) Chem Eng Process 47:1926–1932
11. Mandin Ph, Hamburger J, Bessou S, Picard G (2005) Electrochim Acta 51:1140–1156
12. Mat MD, Aldas K (2005) Int J Hydrog Energy 30:411–420
13. Boissonneau P, Byrne P (2000) J Appl Electrochem 30:767–775
14. Vogt H, Balzer RJ (2005) Electrochim Acta 50:2073–2079
15. Wuthrich R, Comninellis C, Bleuler H (2005) Electrochim Acta 50:5242–5246
16. Gabrielli C, Huet F, Keddam M, Macias A, Sahar A (1989) J Appl Electrochem 19:617–629
17. Dukovic J, Tobias CW (1987) J Electrochem Soc 134:331–343
18. Coenen ELJ, Janssen LJJ (1997) J Appl Electrochem 27:1143–1148
19. Weijs MPMG, Janssen LJJ, Visser GJ (1997) J Appl Electrochem 27:371–378
20. Riegel H, Mitrovic J, Stephan K (1998) J Appl Electrochem 28:10–17
21. Hine F, Murakami K (1980) J Electrochem Soc 127:292–297
22. Funk JE, Thorpe JF (1969) J Electrochem Soc 116:48–54
23. Slavcheva E, Radev I, Bliznakov S, Topalov G, Andreev P, Budevski E (2007) Electrochim Acta 52:3889–3894
24. Grigoriev SA, Porembsky VI, Fateev VN (2006) Int J Hydrog Energy 31:171–175
25. Linkous CA, Anderson HR, Kopitzke RW, Nelson GL (1998) Int J Hydrog Energy 23:525–529
26. Lai Y, Chen Y, Tang Y, Gong D, Chen Z, Lin C (2009) Electrochem Commun 11:2268–2271
27. Kim D, Hwang W, Park HC, Lee KH (2006) J Micromech Microeng 16:2593–2597
28. Zhu LB, Xiu YH, Xu JW, Tamirisa PA, Hess DW, Wong CP (2005) Langmuir 21:11208–11212
29. Fernandez D, Diao Z, Dunne P, Coey JMD (2010) Electrochim Acta 55:8664–8672
30. Matsushima H, Kiuchi D, Fukunaka Y (2009) Electrochim Acta 54:5858–5862
31. Koza JA, Muehlenhoff S, Uhlemann M, Eckert K, Gebert A, Schultz L (2009) Electrochem Commun 11:425–429

32. Koza JA, Uhlemann M, Gebert A, Schultz L (2008) Electrochem Commun 10:1330–1333
33. Iida T, Matsushima H, Fukunaka Y (2007) J Electrochem Soc 154:E112–E115
34. Matsushima H, Kiuchi D, Fukunaka Y, Kuribayashi K (2009) Electrochem Commun 11:1721–1723
35. Mandin Ph, Matsushima H, Fukunaka Y, Wuehrich R, Herrera Calderon E, Lincot D (2008) Journal of the Japanese Society of Microgravity Applications 25:511–515
36. Kiuchi D, Matsushima H, Fukunaka Y, Kuribayashi K (2006) J Electrochem Soc 153:E138–E143
37. Matsushima H, Fukunaka Y, Kuribayashi K (2006) Electrochim Acta 51:4190–4198
38. Matsushima H, Nishida T, Konishi Y, Fukunaka Y, Ito Y, Kuribayashi K (2003) Electrochim Acta 48:4119–4125
39. Li SD, Wang CC, Chen CY (2009) Electrochim Acta 54:3877–3883
40. Wang MY, Wang Z, Guo ZC (2009) Int J Hydrog Energy 34:5311–5317
41. Cheng H, Scott K, Ramshaw C (2002) J Electrochem Soc 149:D172–D177
42. Guelcher SA, Solomentsev YE, Sides PJ, Anderson JL (1998) J Electrochem Soc 145:1848–1855
43. Sides PJ, Tobias CW (1985) J Electrochem Soc 132:583–587
44. Lubetkin S (2002) Electrochim Acta 48:357–375
45. Vogt H (1981) Electrochim Acta 26:1311–1317